



HHS Public Access

Author manuscript

Proc IEEE Int Symp Biomed Imaging. Author manuscript; available in PMC 2023 November 27.

Published in final edited form as:

Proc IEEE Int Symp Biomed Imaging. 2023 April ; 2023: . doi:10.1109/isbi53787.2023.10230729.

AUTOMATED VENTRICLE PARCELLATION AND EVAN'S RATIO COMPUTATION IN PRE- AND POST-SURGICAL VENTRICULOMEGALY

Yuli Wang¹, Anqi Feng¹, Yuan Xue² [Member, IEEE], Lianrui Zuo^{2,3}, Yihao Liu², Ari M. Blitz⁴, Mark G. Luciano⁵, Aaron Carass² [Member, IEEE], Jerry L. Prince^{1,2} [Fellow, IEEE]

¹Department of Biomedical Engineering, Johns Hopkins School of Medicine, USA

²Department of Electrical and Computer Engineering, Johns Hopkins University, USA

³Laboratory of Behavioral Neuroscience, National Institute on Aging, National Institutes of Health, USA

⁴Department of Radiology, Case Western Reserve University School of Medicine, USA

⁵Department of Neurosurgery, Johns Hopkins School of Medicine, USA

Abstract

Normal pressure hydrocephalus (NPH) is a brain disorder associated with enlarged ventricles and multiple cognitive and motor symptoms. The degree of ventricular enlargement can be measured using magnetic resonance images (MRIs) and characterized quantitatively using the Evan's ratio (ER). Automatic computation of ER is desired to avoid the extra time and variations associated with manual measurements on MRI. Because shunt surgery is often used to treat NPH, it is necessary that this process be robust to image artifacts caused by the shunt and related implants. In this paper, we propose a 3D regions-of-interest aware (ROI-aware) network for segmenting the ventricles. The method achieves state-of-the-art performance on both pre-surgery MRIs and post-surgery MRIs with artifacts. Based on our segmentation results, we also describe an automated approach to compute ER from these results. Experimental results on multiple datasets demonstrate the potential of the proposed method to assist clinicians in the diagnosis and management of NPH.

Index Terms—

Normal pressure hydrocephalus; Evan's ratio; Magnetic resonance imaging

1. INTRODUCTION

Normal pressure hydrocephalus (NPH), presenting as ventriculomegaly, is a chronic disease with symptoms of cognitive impairment, gait dysfunction, and dementia [1]. Compared with healthy subjects, the ventricles of NPH patients are greatly expanded with excess cerebrospinal fluid (CSF) causing distortion of the human brain (see Figs. 1(a) and (b)). However, unlike Parkinson's, Alzheimer's, and other neurological diseases, the symptoms of NPH are potentially reversible by CSF valve shunting surgery to remove some excess CSF [2].

The diagnosis of NPH remains challenging because the symptoms of NPH overlap with various forms of dementia. Evan's ratio (ER) [3] as illustrated in Fig. 1(d), is often used to analyze brain magnetic resonance images (MRIs) for possible NPH and to monitor the effectiveness of shunt surgery. To date, the measurements required for computation of ER have been made manually, which is time-consuming and prone to error. In this paper, we describe an automatic procedure, illustrated in Fig. 1(e), which segments and labels the ventricles, measures key dimensions in a normalized space, and outputs the ER.

FreeSurfer [4], RUDOLPH [5], VParNet [6, 7], and several other methods [8–12] provide ventricle segmentations from MRIs. FreeSurfer is an atlas-based approach for whole brain segmentation; it requires long processing time and may fail on NPH subjects with highly enlarged ventricles or post-surgery MRI artifacts [13]. Although RUDOLPH is specially designed for subjects with enlarged ventricles, it has a multi-hour run time and often fails on post-surgical subjects. VParNet uses a 3D U-net to perform ventricle segmentation in about 2 minutes. It works well on both NPH and healthy subjects, but it also fails when MRI artifacts are present (see Fig. 4(c)).

In this paper, we propose a novel ventricle segmentation algorithm based on localization network and a modified 3D U-net [14]. The method first finds a region-of-interest (ROI) for the ventricles systems. The ROIs are then used to restrict the area of interests of a follow-up segmentation model such that it can focus on the ventricle regions and ignore outer regions that sometimes affected by image artifacts. We conducted comprehensive experiments on three datasets: one dataset with healthy controls, one dataset of NPH patients, and one dataset of NPH subjects with post-surgery implants (PS-NPH). Our method consistently outperformed existing methods, especially on subjects with MRI artifacts. Built upon the successful segmentation of ventricles, we then propose an automated ER computation method and validated the agreement of the automated results with manual calculations on 101 subjects. The correlation between our manual and automated ER computations was 0.983, indicating the high reliability of our proposed ER calculation framework. Our contributions can be summarized as: 1) First automated computation of Evan's ratio; 2) Validated Evan's ratio on 101 subjects; 3) Improved ventricle segmentation that is robust to post surgical artifacts.

2. METHODS

An overview of our method is shown in Fig. 2. To avoid the effect of MRI artifacts in the image, we use a 3D locating network as the first step; this also reduces the area of interest and thus the complexity of the task in the subsequent steps. The locating network uses the architecture in [15] and is designed to generate four separate 3D bounding boxes, two for the left and right lateral ventricles and one each for the third and fourth ventricles. We use instance normalization with a small batch size for memory efficient training of the locating network on 3D volumes. The segmentation network is based on the 3D U-net [14] with instance normalization and nearest-neighbor interpolation for upsampling. It takes the ROI-cropped images as input and segments the left lateral (LLV), right lateral (RLV), third (3V), and fourth (4V) ventricles. The cerebral aqueduct is included in the third ventricle label.

3D locating network:

For the locating network, all images were rigidly registered to a standard MNI space. The ground truth bounding boxes were obtained from the manual delineations of the four ventricles, where the maximum and minimum coordinates were used as the starting and stopping coordinates of the bounding box. The loss function to train the locating network is given by

$$\mathcal{L}_{\text{box}} = \frac{1}{N} \sum_{i=1}^N s(\hat{x}_i - x_i), \text{ where}$$

$$s(u) = \begin{cases} 0.5u^2 & \text{if } |u| < 1, \\ |u| - 0.5 & \text{otherwise.} \end{cases}$$

Here, \hat{x}_i is a predicted bounding box coordinate with corresponding ground truth x_i . There are $N=24$, which corresponds to the two vertices for each of the four desired bounding boxes. Our locating network was trained for 500 epochs using the Adam optimization algorithm with a learning rate of $\alpha = 10^{-3}$.

Ventricle parcellation network:

The locating network finds four tight bounding boxes of varying sizes. To accommodate our parcellation network, we expand the bounding boxes symmetrically in all six cardinal directions so that each dimension is a multiple of 32. The segmentation network is trained with the loss

$$\mathcal{L}_{\text{Dice}} = \left(1 - \frac{1}{L} \sum_{l=1}^L \frac{\epsilon + 2 \sum_v M_{vl} N_{vl}}{\epsilon + \sum_v M_{vl} + \sum_v N_{vl}} \right),$$

where M_{vl} is the probability that voxel v has label l generated by the network after a softmax, N_{vl} is the binary value indicating if voxel v should be labeled l . $\epsilon = 10^{-3}$ is used to avoid a zero denominator during training. Data augmentation during training includes random left-right flipping, elastic deformation, and rotation. Our network was trained for 150 epochs using the Adam optimizer with a learning rate of $\alpha = 10^{-3}$.

Automated Evan's ratio calculation:

Based on our ventricle segmentation result and using a brain mask from [16], we automated the Evan's ratio (ER) calculation as illustrated in Fig. 1(f). Recall that all images and corresponding masks are in MNI space. ER is calculated as the maximum width of the frontal horns (MWFH) from the lateral ventricle masks divided by the maximum width of the inner skull (MWS). Both the MWFH and MWS are identified as horizontal lines in MNI space, as such we simply search our lateral ventricle masks for the MWFH, and the skull mask for the MWS.

3. EXPERIMENTS AND RESULTS

Datasets and Pre-processing:

Magnetization-prepared rapid gradient-echo (MPRAGE) T1-weighted (T1-w) images from three cohorts were used to train and validate our proposed method. Four ventricle compartments—i.e., the LLV, RLV, 3V, and 4V—were manually delineated. The first dataset contains 50 MRIs of healthy controls from Neuromorphometrics Inc. (NMM) [17]; from these, 15 images were randomly selected for training, 5 for validation, and the remaining 30 were used for testing. The second dataset contains 95 NPH subjects [7]; of these, 25 images were used for training, 5 for validation, and the remaining 65 for testing. The third cohort contains 6 post-surgical images; these we used exclusively for testing. All images were pre-processed using N4 inhomogeneity correction [18] and rigid registration to MNI space.

In our first experiment, we compare our proposed method to FreeSurfer [4] and VParNet [7] on the 30 testing subjects from the NMM cohort, 65 subjects from our NPH cohort, and 6 post-surgery subjects. We computed the Dice similarity coefficient (DSC) and the 95% Hausdorff distance (HD) for these three datasets, and report results in Fig. 3. For all three cohorts, our proposed method is significantly better than VParNet based on the Wilcoxon signed-rank test (see Fig. 3 for significance levels). A visualization of the ventricle parcellation produced by our method is shown in Figs. 4 (a), (b), and (c) for the NMM, NPH, and PS-NPH data, respectively. As illustrated in Fig. 4 (c), FreeSurfer and VParNet both have failure cases in the area of the post-surgery valve artifact.

In our second experiment, we compare the Evan's ratio (ER) value from our method with the ER identified by manual measurements on the same testing subjects as in our parcellation experiment (30 NMM subjects, 65 NPH subjects, and 6 PS-NPH subjects). The manual measurements of ER were obtained by averaging the ER determined by two annotators. Figure 5 shows a scatter plot of our automatic results and the manual measurements; the correlation coefficient between these two measurements is 0.983. The mean difference between the automated and manual measurements is 0.008 (1.4%). We note that the automated and manual measurements of ER separated the healthy subjects (NMM cohort) and NPH subjects (NPH and PS-NPH cohorts) at a threshold of 0.3, which coincides with the threshold used by clinicians for NPH diagnosis [1, 19].

4. CONCLUSIONS

In this paper, we proposed a cascade workflow to regulate multi-ROIs for robust parcellation of ventricles in subjects with normal and enlarged ventricles, as well as those with post-surgery MRI artifacts. Compared with the current state-of-the-art methods, our method achieves superior results in both qualitative and quantitative evaluations on three datasets. In addition, our proposed method is the only one that handled patients with post-surgery images containing artifacts, demonstrating the robustness of the proposed ROI-aware segmentation. We also presented an automated ER calculation method to assist with diagnosis and monitoring of NPH. The correlation coefficient of ER between our automatic and the manual measurement was 0.983, demonstrating the clinical potential of our method.

ACKNOWLEDGMENTS

This work was supported in part by the NIH / NINDS under grant U01-NS122764 (PI: M.G. Luciano) and in part by the Intramural Research Program of the NIH, National Institute on Aging. Portions of the used data in this study was conducted retrospectively using human subject data made available by Neuromorphometrics Inc. Ethical approval was not required as confirmed by the license attached with this data. The remainder of the data was acquired in line with the principles of the Declaration of Helsinki. Approval was granted by an IRB Committee of the Johns Hopkins School of Medicine with approval IDs CIR00002740 (approved June 6, 2014) and IRB00305245 (approved January 13, 2022).

References

- [1]. Shprecher D, Schwalb J, and Kurlan R, “Normal pressure hydrocephalus: diagnosis and treatment,” *Current neurology and neuroscience reports*, vol. 8, no. 5, pp. 371–376, 2008. [PubMed: 18713572]
- [2]. Stein SC, Burnett MG, and Sonnad SS, “Shunts in normal-pressure hydrocephalus: do we place too many or too few?,” *Journal of Neurosurgery*, vol. 105, no. 6, pp. 815–822, 2006. [PubMed: 17405250]
- [3]. Brix MK, Westman E, Simmons A, Ringstad GA, Eide PK, Wagner-Larsen K, Page CM, Vitelli V, and Beyer MK, “The Evans’ Index revisited: New cut-off levels for use in radiological assessment of ventricular enlargement in the elderly,” *European Journal of Radiology*, vol. 95, pp. 28–32, 2017. [PubMed: 28987681]
- [4]. Fischl B, “FreeSurfer,” *NeuroImage*, vol. 62, no. 2, pp. 774–781, 2012. [PubMed: 22248573]
- [5]. Carass A, Shao M, Li X, Dewey BE, Blitz AM, Roy S, Pham DL, Prince JL, and Ellingsen LM, “Whole brain parcellation with pathology: Validation on ventriculomegaly patients,” in *International Workshop on Patch-Based Techniques in Medical Imaging*, 2017, pp. 20–28.
- [6]. Shao M, Han S, Carass A, Li X, Dewey BE, Blitz AM, Prince JL, and Ellingsen LM, “Shortcomings of Ventricle Segmentation Using Deep Convolutional Networks,” in *Understanding and Interpreting Machine Learning in Medical Image Computing Applications. MLCN 2018, DLF 2018, IMIMIC 2018*. 2018, vol. 11038 of *Lecture Notes in Computer Science*, pp. 79–86, Springer Berlin Heidelberg.
- [7]. Shao M, Han S, Carass A, Li X, Blitz AM, Shin J, Prince JL, and Ellingsen LM, “Brain ventricle parcellation using a deep neural network: Application to patients with ventriculomegaly,” *NeuroImage: Clinical*, vol. 23, pp. 101871, 2019. [PubMed: 31174103]
- [8]. Shiee N, Bazin P-L, Cuzzocreo JL, Blitz A, and Pham DL, “Segmentation of brain images using adaptive atlases with application to ventriculomegaly,” in *22nd Inf. Proc. in Med. Imaging (IPMI 2011)*. 2011, vol. 6801 of *Lecture Notes in Computer Science*, pp. 1–12, Springer Berlin Heidelberg.
- [9]. Ellingsen LM, Roy S, Carass A, Blitz AM, Pham DL, and Prince JL, “Segmentation and labeling of the ventricular system in normal pressure hydrocephalus using patch-based tissue classification and multi-atlas labeling,” in *Proceedings of SPIE Medical Imaging (SPIE-MI 2016)*, San Diego, CA, February 27 – March 3, 2016, 2016, vol. 9784, pp. 97840G–97840G–7.
- [10]. Atlason HE, Shao M, Robertsson V, Sigurdsson S, Gudnason V, Prince JL, and Ellingsen LM, “Large-scale parcellation of the ventricular system using convolutional neural networks,” in *Proceedings of SPIE Medical Imaging (SPIE-MI 2019)*, San Diego, CA, February 16 – 21, 2019, 2019, vol. 10953, pp. 111–117.
- [11]. Wang Y, Feng A, Xue Y, Shao M, Blitz AM, Luciano MG, Carass A, , and Prince JL, “Investigation of probability maps in deep-learning-based brain ventricle parcellation,” in *Proceedings of SPIE Medical Imaging (SPIE-MI 2023)*, San Diego, CA, February 19 – 23, 2023, 2023.
- [12]. Zhou P, Liu Z, Wu H, Wang Y, Lei Y, and Abbaszadeh S, “Automatically detecting bregma and lambda points in rodent skull anatomy images,” *PloS one*, vol. 15, no. 12, pp. e0244378, 2020. [PubMed: 33373400]
- [13]. Lemcke J, Meier U, Müller C, Fritsch MJ, Kehler U, Langer N, Kiefer M, Eymann R, Schuhmann MU, Speil A, et al. , “Safety and efficacy of gravitational shunt valves in patients

- with idiopathic normal pressure hydrocephalus: a pragmatic, randomised, open label, multicentre trial (svasona),” *Journal of Neurology, Neurosurgery & Psychiatry*, vol. 84, no. 8, pp. 850–857, 2013. [PubMed: 23457222]
- [14]. Çiçek Ö, Abdulkadir A, Lienkamp SS, Brox T, and Ronneberger O, “3D U-Net: learning dense volumetric segmentation from sparse annotation,” in *19th International Conference on Medical Image Computing and Computer Assisted Intervention (MICCAI 2016)*. Springer, 2016, pp. 424–432.
- [15]. Han S, Carass A, He Y, and Prince JL, “Automatic cerebellum anatomical parcellation using U-Net with locally constrained optimization,” *NeuroImage*, vol. 218, pp. 116819, 2020. [PubMed: 32438049]
- [16]. Roy S, Butman JA, Pham DL, Alzheimers Disease Neuroimaging Initiative, et al. , “Robust skull stripping using multiple MR image contrasts insensitive to pathology,” *Neuroimage*, vol. 146, pp. 132–147, 2017. [PubMed: 27864083]
- [17]. Marcus DS, Wang TH, Parker J, Csernansky JG, Morris JC, and Buckner RL, “Open Access Series of Imaging Studies (OASIS): cross-sectional MRI data in young, middle aged, nondemented, and demented older adults,” *Journal of cognitive neuroscience*, vol. 19, no. 9, pp. 1498–1507, 2007. [PubMed: 17714011]
- [18]. Tustison NJ, Avants BB, Cook PA, Zheng Y, Egan A, Yushkevich PA, and Gee JC, “N4ITK: Improved N3 Bias Correction,” *IEEE Trans. Med. Imag.*, vol. 29, no. 6, pp. 1310–1320, 2010.
- [19]. Zhou X and Xia J, “Application of Evans Index in Normal Pressure Hydrocephalus Patients: A Mini Review,” *Frontiers in Aging Neuroscience*, vol. 13, 2021.

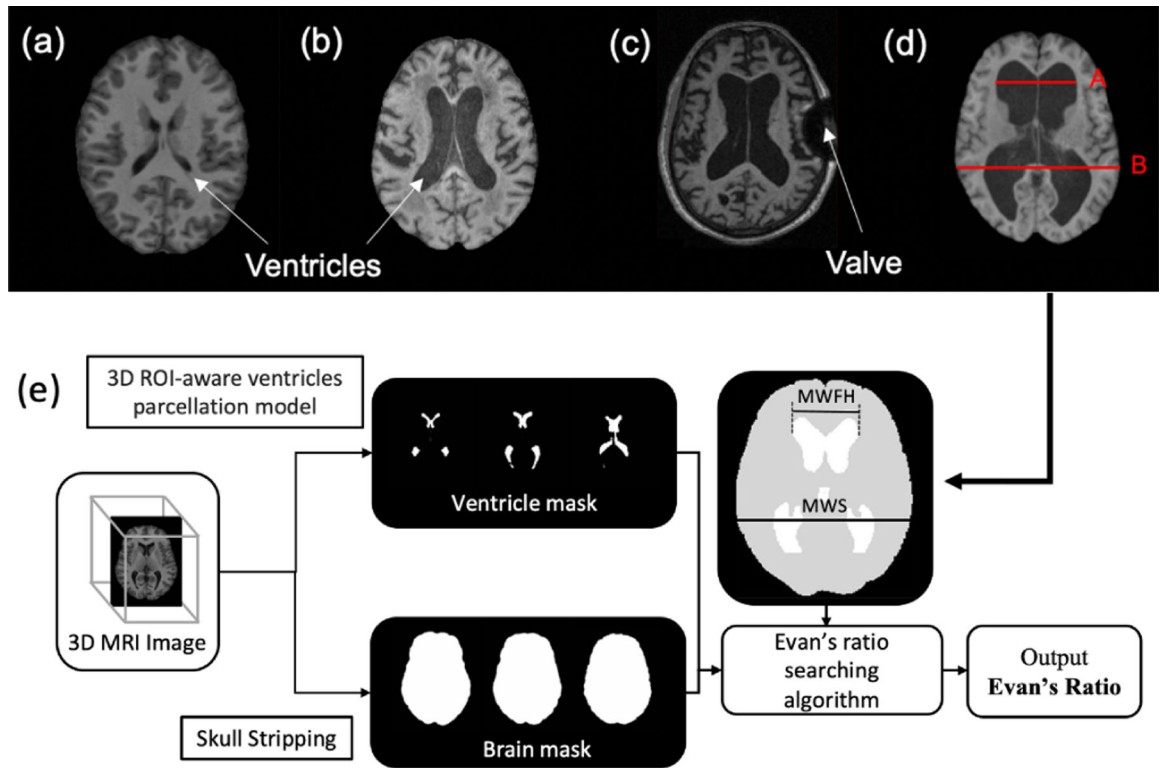


Fig. 1.

T1-weighted MRIs showing the lateral ventricles of: (a) a healthy subject, (b) an NPH subject, and (c) a post-surgical subject with an MRI artifact. (d) Evan's ratio is A/B . (e) Flowchart of automated Evan's ratio computation, including the measurement of maximum width of frontal horns (MWFH) and maximum width of inner skull (MWS).

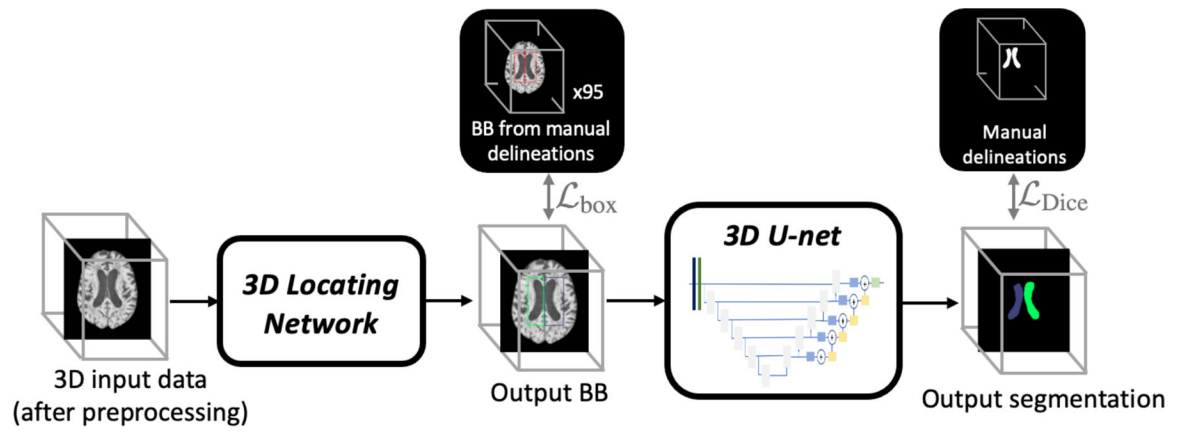


Fig. 2. Flowchart of our ventricle parcellation. The locating network finds a 3D ROI around the ventricles system, then the segmentation network segments the primary ventricle cavities. BBs refer to bounding boxes.

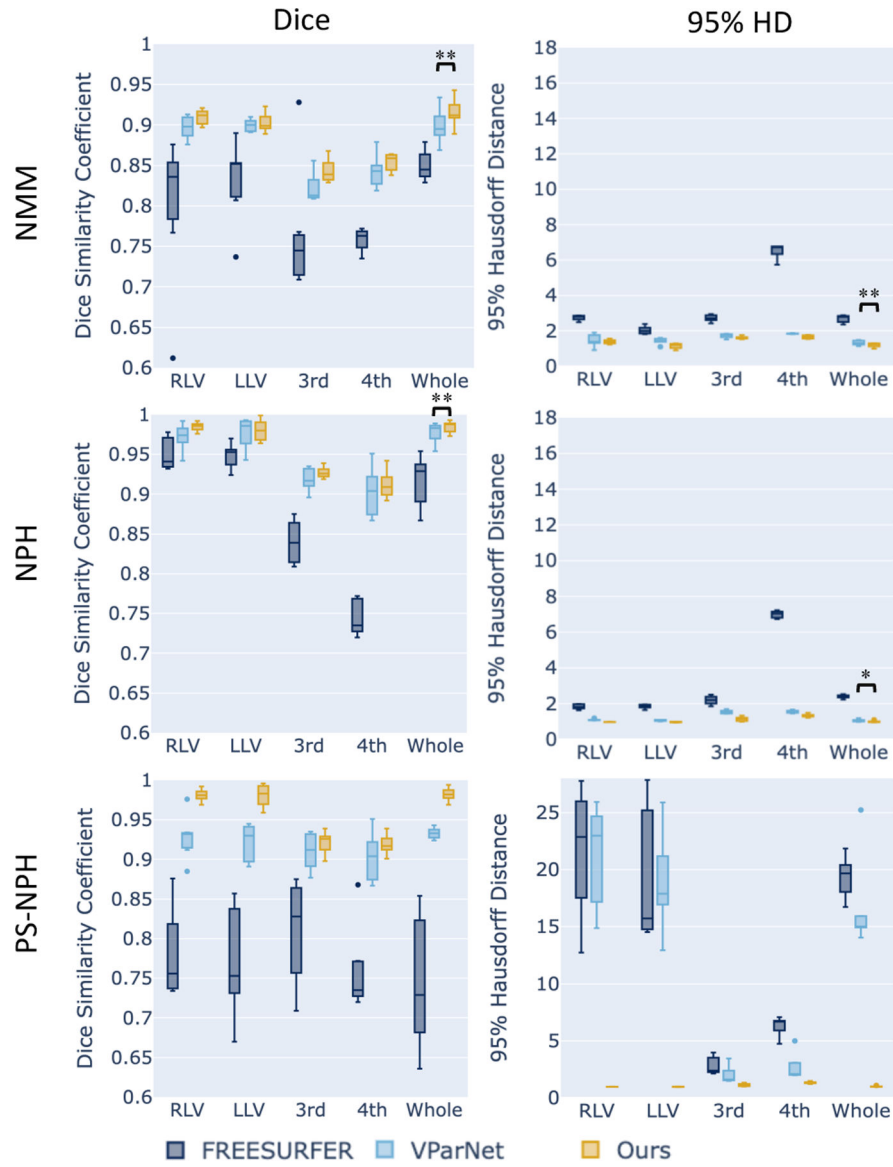


Fig. 3. Box plots of DSC and 95% HD on NMM, NPH, and PS-NPH test datasets. Wilcoxon signed-rank test was conducted between VParNet and our method. Our results were significantly better in all datasets (marked by asterisks: * for $p < 0.05$ and ** for $p < 0.01$.)

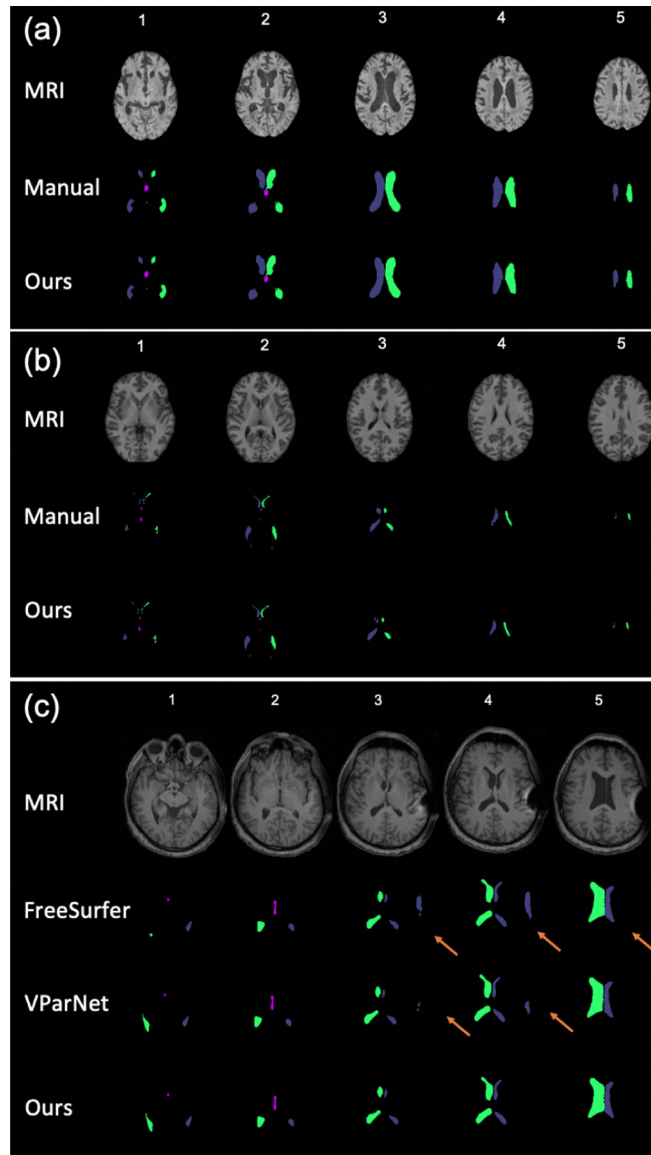


Fig. 4. Comparison of three methods for (a) an NMM, (b) an NPH, and (c) a PS-NPH subject; five slices for each subject.

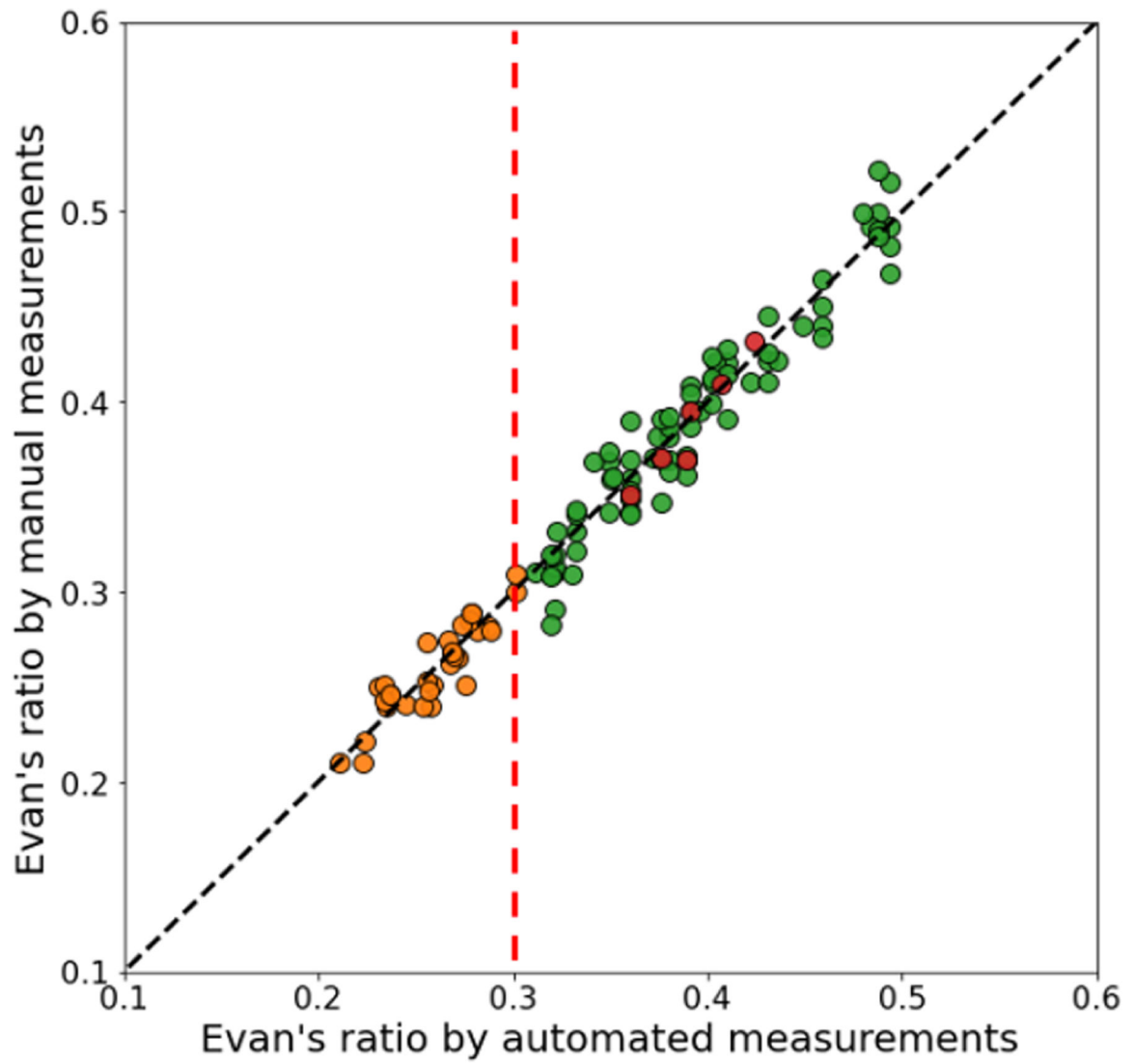


Fig. 5. Comparison of Evan's ratio between the automated calculation and the manual measurement.